Data report: clay mineral assemblages in slope basin sediments and mass-transport deposits at Sites C0018 and C0021, IODP Expeditions 333 and 338[1]

Michael B. Underwood[2]

Chapter contents

Abstract 1
Introduction 1
Methods 2
Results 3
Acknowledgments 4
References 4
Figures 6
Tables 10

[1]Underwood, M.B., 2017. Data report: clay mineral assemblages in slope basin sediments and mass-transport deposits at Sites C0018 and C0021, IODP Expeditions 333 and 338. *In* Strasser, M., Dugan, B., Kanagawa, K., Moore, G.F., Toczko, S., Maeda, L., and the Expedition 338 Scientists, *Proceedings of the Integrated Ocean Drilling Program,* 338: Yokohama (Integrated Ocean Drilling Program). doi:10.2204/iodp.proc.338.207.2017
[2]Department of Earth and Environmental Science, New Mexico Institute of Mining and Technology, Socorro New Mexico 87801, USA. UnderwoodM@missouri.edu

Abstract

This report summarizes the results of X-ray diffraction analyses of core samples from Sites C0018 and C0021 in the Nankai subduction zone (offshore southwest Japan). The Integrated Ocean Drilling Program recovered the cores during Expeditions 333 and 338, and a total of 122 specimens were analyzed (<2 mm size fraction). Depositional facies include trench slope deposits (hemipelagic mud with thin interbeds of turbidites and volcanic ash), mass-transport deposits (MTD), and sand-rich slope basin deposits. Illite is generally the most abundant clay mineral within both intact and MTD intervals. At Site C0018, the average amount of illite in the clay-size fraction of Subunit Ia (slope basin with MTD) is 37.7 wt% (standard deviation = 4.2). Proportions of smectite and chlorite average 26.8 and 20.2 wt%, respectively. Average contents of kaolinite and quartz are 4.1 and 11.3 wt%, respectively. Within Subunit Ib (sandy slope basin), the average contents are 37.2 wt% illite, 23.6 wt% smectite, 30.7 wt% undifferentiated chlorite + kaolinite, and 8.5 wt% quartz. Results are similar at Site C0021, where illite averages 43.7 wt% (standard deviation = 4.5). Average values for the other minerals are 23.6 wt% smectite, 24.3 wt% undifferentiated chlorite + kaolinite, and 8.4 wt% quartz. Most values of illite/smectite expandability fall between 55% and 65%. Values of the illite crystallinity index are indicative of detrital sources that were exposed to anchizone and epizone metamorphic conditions.

Introduction

The Nankai Trough Seismogenic Zone Experiment (NanTroSEIZE) has grown over several years to become the most comprehensive ocean drilling transect in any subduction system (Ashi et al., 2009; Screaton et al., 2009; Tobin et al., 2009; Underwood et al., 2010; Expedition 333 Scientists, 2012a; Tobin et al., 2015; also see the **"Expedition 338 summary"** chapter [Strasser et al., 2014a]). Expeditions 333 and 338 of the Integrated Ocean Drilling Program (IODP) cored at Sites C0018 and C0021 (Fig. **F1**). Mass-transport deposits (MTDs) are common at both sites, which are located in a trench-slope basin immediately downslope of a megasplay fault in the accretionary prism (Fig. **F2**). Site C0021 is located ~2 km northwest of Site C0018 in a more proximal position for the MTDs (Fig. **F2**). The primary drilling objectives were to establish a

doi:10.2204/iodp.proc.338.207.2017

Quaternary mass-movement event stratigraphy with good age control and to sample an exceptionally thick MTD complex for subsequent analyses of the sediments' rheological behavior.

The dominant lithology at Sites C0018 and C0021 is clayey silt to silty clay (hemipelagic mud). Calcium carbonate contents are relatively high in the mud due to elevation of the slope basin above the calcite compensation depth. Depositional ages, based on nannofossil events and paleomagnetic datums, are younger than 1.46 Ma (Expedition 333 Scientists, 2012b; also see the "Site C0021" chapter [Strasser et al., 2014b]). Thin interbeds of silt- to sand-size volcanic ash are abundant, as are silty to sandy turbidites. A lithologic boundary between Subunits Ia and Ib was recognized based on the prevalence of sand beds (more sand in Subunit Ib). That boundary occurs at 190.65 meters below seafloor (mbsf) at Site C0018 and at 176.17 mbsf at Site C0021 (Fig. F3).

MTDs occur within Subunit Ia. Visual evidence from the split cores for mass-transport mechanisms (e.g., submarine slides and debris flows) includes convolute and tilted strata, intervals of remobilized mud clasts overlying tilted strata, and internal shear zones. Those observations were bolstered by 3-D analyses of X-ray CT scans. The thicker MTD intervals comprise a mixture of mud-rich debrites, intact hemipelagic layers, and convoluted banded deposits denoting extensive deformation within the interior of the failure.

This report documents the results of X-ray diffraction (XRD) analyses of 122 core samples from Sites C0018 and C0021. The report's primary objective is to provide compositional data from the slope basin deposits and MTDs for comparisons with other sites and tectonostratigraphic units along the NanTroSEIZE transect (e.g., Guo and Underwood, 2012; Underwood and Guo, 2013).

Methods

Sample preparation

Most of the samples analyzed in this study came from "clusters" that included companion specimens for shipboard bulk-powder XRD, X-ray fluorescence, moisture and density, and carbon-carbonate. The clusters were positioned next to sampling intervals for whole rounds, including those extracted for interstitial water. Shipboard XRD scans provided estimates of the relative abundance of total clay minerals, quartz, feldspar, and calcite (see the "Site C0018" chapter [Expedition 333 Scientists, 2012b], and the "Site C0021" chapter [Strasser et al., 2014b]).

Clay-size fractions were isolated for XRD analyses by air-drying and gentle hand-crushing of the mud with mortar and pestle, after which specimens were immersed in 3% H_2O_2 for at least 24 h to digest organic matter. To prevent flocculation, ~250 mL of Na-hexametaphosphate solution (4 g/1000 mL distilled H_2O) was added, and beakers were inserted into an ultrasonic bath for several minutes to promote disaggregation. That step (and additional soaking) was repeated until visual inspection indicated complete disaggregation. Washing consisted of two passes through a centrifuge (8200 rpm for 25 min; ~6000 g) with resuspension in distilled deionized water after each pass. After transferring the suspended sediment to a 60 mL plastic bottle, each specimen was resuspended by vigorous shaking and a 2 min application of an ultrasonic cell probe. A centrifuge was used to separate the clay-size splits (<2 µm equivalent spherical settling diameter; 1000 rpm for 2.4 min; ~320 g). Preparation of oriented clay aggregates followed the filter-peel method (Moore and Reynolds, 1989) using 0.45 µm filter membranes. A closed vapor chamber was used to saturate clay aggregates with ethylene glycol heated to 60°C for at least 24 h prior to XRD analysis.

X-ray diffraction

Two X-ray diffractometers were used to analyze clay-size specimens. When the project began, the XRD laboratory at the University of Missouri was equipped with a Scintag Pad V X-ray diffractometer with CuKα radiation (1.54 Å) and Ni filter. Those scans of oriented clay aggregates were run at 40 kV and 30 mA over a scanning range of 3° to 26.5°2θ, a rate of 1°2θ/min, and a step size of 0.01°2θ. Slits were 0.5 mm (divergence) and 0.2 mm (receiving). The Department of Geological Sciences shut down that facility before NanTroSEIZE research was finished, so the remaining samples (including all samples from Site C0021) were analyzed at the New Mexico Bureau of Geology and Mineral Resources using a Panalytical X'Pert Pro diffractometer with Cu anode. We ran those continuous scans at generator settings of 45 kV and 40 mA over an angular range of 3° to 26.5°2θ, with scan step time of 1.6 s and step size of 0.01°2θ. Slits are 1.0 mm (divergence) and 0.1 mm (receiving) and the sample holder spinning. MacDiff software (version 4.2.5) was utilized to draw a baseline of intensity, smooth counts, correct peak positions offset by misalignment of the detector (using the quartz [100] peak at 20.95°2θ; d-value = 4.24 Å), and calcu-

late integrated peak area (total counts) and peak width at half height (Δ°2θ).

Calculations of mineral abundance

To achieve the best possible accuracy, XRD methods require calibration with internal standards, use of single-line reference intensity ratios, and some fairly elaborate sample preparation steps to create optimal random particle orientations (e.g., Środoń et al., 2001; Omotoso et al., 2006). Given the unusually large number of samples throughout the NanTroSEIZE project, our priority has been to obtain reliable semiquantitative accuracy with optimal efficiency. To accomplish that for the clay-size fraction, standard mineral mixtures (smectite + illite + chlorite + quartz) were analyzed as described by Underwood et al. (2003), and a matrix of normalization factors was computed using singular value decomposition (SVD). We record the integrated areas of a broad smectite (001) peak centered at ~5.3°2θ (d-value = 16.5 Å), the illite (001) peak at ~8.9°2θ (d-value = 9.9 Å), the composite chlorite (002) + kaolinite (001) peak at 12.5°2θ (d-value = 7.06 Å), and the quartz (100) peak at 20.85°2θ (d-value = 4.26 Å). Because of differences in X-ray tubes and diffractometers, it was necessary to solve for three sets of normalization factors (Table **T1**) and then employ them during computations. Average errors using this method are 3.9% for smectite, 1.0% for illite, 1.9% for chlorite, and 1.6% for quartz. The chlorite (002) and kaolinite (001) peaks overlap almost completely, so a refined version of the Biscaye (1964) method was used to discriminate kaolinite (002) from chlorite (004), as documented by Guo and Underwood (2011). The average error of accuracy for the chlorite/kaolinite ratio is 2.6%. That ratio was used to compute individual mineral percentages from the SVD weight percent of undifferentiated chlorite (002) + kaolinite (001).

To calculate the abundance of individual clay minerals in the bulk sediment, each relative weight percent value among the clay minerals (where smectite + illite + chlorite + kaolinite = 100%) was multiplied by the weight percent of total clay minerals within the bulk powder (where total clay minerals + quartz + feldspar + calcite = 100%), as determined by shipboard XRD analyses of collocated specimens (Expedition 333 Scientists, 2012b; also see the **"Site C0021"** chapter [Strasser et al., 2014b]). To facilitate direct comparisons with other published data sets from the region, tabulations include the weighted peak-area percentages for smectite, illite, and undifferentiated chlorite + kaolinite using Biscaye (1965) weighting factors (1 × smectite, 4 × illite, and 2 × chlorite + kaolinite). Errors of accuracy using that method can be substantially greater (±10% or more) as compared to the errors using SVD factors (Underwood et al., 2003).

For documentation of clay diagenesis, the saddle/peak method of Rettke (1981) was used to calculate percent expandability of smectite and illite/smectite (I/S) mixed-layer clay. This method is sensitive to the proportions of discrete illite (I) versus I/S mixed-layer clay; the curve for 1:1 mixtures of I and I/S provides the best match for the range of Nankai specimens. Values of the illite crystallinity (Kübler) index are reported here as peak width at half height (Δ°2θ) for the (001) reflection; the illite peak typically narrows as levels of thermal maturity increase.

Results

Tables **T2** and **T3** show the peak-area values (total counts) for common minerals in the clay-size fraction, segregated by lithologic unit. Tables **T2** and **T3** also include the values of mineral abundance calculated with SVD normalization factors and weighted peak area (%) using Biscaye (1965) factors. Values are rounded to the nearest 1 wt% in acknowledgment of the statistical disadvantages of having to use three sets of SVD normalization factors. In addition, some of these results suffer from unusually low peak intensities caused by relatively high concentrations of biogenic calcite in the clay-size fraction (Table **T2**).

Site C0018

Detrital illite is the most abundant clay mineral in the slope basin deposits, followed by detrital smectite. The relative abundance of illite within Subunit Ia ranges from 32 to 46 wt% (Fig. **F3**) with a mean value (μ) of 37.7 wt% and a standard deviation (σ) of 4.2. The amount of smectite in the clay-size fraction ranges from 14 to 38 wt% (μ = 26.8; σ = 5.1). Percentages of chlorite range from 12 to 36 wt% (μ = 20.2; σ = 3.8). Percentages of clay-size kaolinite and quartz are subordinate, averaging 4.1 wt% (σ = 3.4) and 11.3 wt% (σ = 4.7), respectively. There are no obvious differences in composition between intact hemipelagic deposits and MTDs.

The clay minerals in samples from Subunit Ib are similar to those in overlying deposits (Fig. **F3**). The range of relative percentages for illite is from 30 to 47 wt% (μ = 37.2; σ = 5.3), whereas smectite varies from 8 to 39 wt% (μ = 23.6; σ = 7.2). For 6 specimens, it was impossible to resolve the chlorite/kaolinite ratio because of interference by a strong barite peak (Table **T2**). The average value for undifferentiated chlorite + kaolinite is 30.7 wt%, and the average for clay-size quartz is 8.5 wt%.

Figure F4 illustrates how abundances of smectite and illite within the bulk sediment change as a function of depth. Smectite is probably the most influential for modulating frictional and geotechnical properties of the sediment. Within Subunit Ia, bulk sediment smectite ranges from 8 to 18 wt% (μ = 13.8; σ = 2.6). Comparable values within Subunit Ib range from 3 to 22 wt% (μ = 12.6; σ = 4.6).

Illite crystallinity (Kübler) index values for strata within Subunit Ia range from 0.26 to 0.42Δ°2θ (μ = 0.33Δ°2θ). The results from Subunit Ib are basically the same (μ = 0.33Δ°2θ), with no systematic changes as a function of depth (Fig. F4). As a frame of reference, the boundary between advanced diagenesis and anchizone metamorphism is set at 0.52Δ°2θ, and the achizone/epizone boundary (incipient greenschist facies) coincides with 0.32Δ°2θ (Warr and Mählmann, 2015). Deposits from Subunit Ia yield I/S expandability values that range from 48 to 68 wt% (μ = 61%), with no systematic changes as a function of depth (Fig. F4). The average value of I/S expandability for Subunit Ib is 64%.

Site C0021

The 21 specimens analyzed from Site C0021 (1 replicate) are limited to Subunit Ia and reveal clay mineral assemblages similar to those from Subunit Ia at Site C0018 (Fig. F3). Some of these results also suffer from unusually low peak intensities caused by relatively high concentrations of biogenic calcite (Table T3). The relative abundance of illite in the clay-size fraction ranges from 39 to 52 wt% (μ = 43.7; σ = 4.5). Smectite abundance ranges from 15 to 38 wt% (μ = 23.6; σ = 5.2). Chlorite remains consistently subordinate, ranging from 9 to 27 wt% (μ = 19.5; σ = 4.5), whereas clay-size kaolinite (μ = 4.8; σ = 3.8) and quartz (μ = 8.4; σ = 5.3) remain consistently low. Calculated values of smectite in bulk sediment (Fig. F4) range from 7 to 22 wt% (μ = 11.7, σ = 3.2). Illite crystallinity (Kübler) index values range from 0.21 to 0.42Δ°2θ (Fig. F4), with an average value of 0.35Δ°2θ (i.e., mostly anchizone source rocks). The expandability of I/S clays ranges from 49% to 66%, with an average value of 58%.

Acknowledgments

This research used samples provided by the Integrated Ocean Drilling Program (IODP). We thank the Mantle Quest Japan drilling crew, Marine Works Japan laboratory technicians, and scientists aboard D/V *Chikyu* for their dedicated assistance during IODP Expeditions 333 and 338. Funding was granted by the Consortium for Ocean Leadership, U.S. Science Support Program (task orders T333B58 and T338B58). N. Walla, J. Guo, K. Ekinci, and C. Song assisted with sample preparation. The manuscript was reviewed by Tania Villaseñor.

References

Ashi, J., Lallemant, S., Masago, H., and the Expedition 315 Scientists, 2009. Expedition 315 summary. *In* Kinoshita, M., Tobin, H., Ashi, J., Kimura, G., Lallemant, S., Screaton, E.J., Curewitz, D., Masago, H., Moe, K.T., and the Expedition 314/315/316 Scientists, *Proceedings of the Integrated Ocean Drilling Program,* 314/315/316: Washington, DC (Integrated Ocean Drilling Program Management International, Inc.). **http://dx.doi.org/10.2204/iodp.proc.314315316.121.2009**

Biscaye, P.E., 1964. Distinction between kaolinite and chlorite in recent sediments by X-ray diffraction. *American Mineralogist,* 49:1281–1289. **http://www.minsocam.org/ammin/AM49/AM49_1281.pdf**

Biscaye, P.E., 1965. Mineralogy and sedimentation of recent deep-sea clay in the Atlantic Ocean and adjacent seas and oceans. *Geological Society of America Bulletin,* 76(7):803–831. **http://dx.doi.org/10.1130/0016-7606(1965)76[803:MASORD]2.0.CO;2**

Expedition 333 Scientists, 2012a. Expedition 333 summary. *In* Henry, P., Kanamatsu, T., Moe, K., and the Expedition 333 Scientists, *Proceedings of the Integrated Ocean Drilling Program,* 333: Tokyo (Integrated Ocean Drilling Program Management International, Inc.). **http://dx.doi.org/10.2204/iodp.proc.333.101.2012**

Expedition 333 Scientists, 2012b. Site C0018. *In* Henry, P., Kanamatsu, T., Moe, K., and the Expedition 333 Scientists, *Proceedings of the Integrated Ocean Drilling Program,* 333: Tokyo (Integrated Ocean Drilling Program Management International, Inc.). **http://dx.doi.org/10.2204/iodp.proc.333.103.2012**

Guo, J., and Underwood, M.B., 2011. Data report: refined method for calculating percentages of kaolinite and chlorite from X-ray diffraction data, with application to the Nankai margin of southwest Japan. *In* Kinoshita, M., Tobin, H., Ashi, J., Kimura, G., Lallemant, S., Screaton, E.J., Curewitz, D., Masago, H., Moe, K.T., and the Expedition 314/315/316 Scientists, *Proceedings of the Integrated Ocean Drilling Program,* 314/315/316: Washington, DC (Integrated Ocean Drilling Program Management International, Inc.). **http://dx.doi.org/10.2204/iodp.proc.314315316.201.2011**

Guo, J., and Underwood, M.B., 2012. Data report: clay mineral assemblages from the Nankai Trough accretionary prism and the Kumano Basin, IODP Expeditions 315 and 316, NanTroSEIZE Stage 1. *In* Kinoshita, M., Tobin, H., Ashi, J., Kimura, G., Lallemant, S., Screaton, E.J., Curewitz, D., Masago, H., Moe, K.T., and the Expedition 314/315/316 Scientists, *Proceedings of the Integrated Ocean Drilling Program,* 314/315/316: Washington, DC (Integrated Ocean Drilling Program Management International, Inc.). **http://dx.doi.org/10.2204/iodp.proc.314315316.202.2012**

Moore, D.M., and Reynolds, R.C., Jr., 1989. Sample preparation techniques for clay minerals. *In* Moore, D.M., and Reynolds, R.C., Jr. (Eds.), *X-Ray Diffraction and the Identification and Analysis of Clay Minerals:* New York (Oxford Univ. Press USA), 179–201.

Omotoso, O., McCarty, D.K., Hillier, S., and Kleeberg, R., 2006. Some successful approaches to quantitative mineral analysis as revealed by the 3rd Reynolds Cup contest. *Clays and Clay Minerals,* 54(6):748–760. **http://dx.doi.org/10.1346/CCMN.2006.0540609**

Rettke, R.C., 1981. Probable burial diagenetic and provenance effects on Dakota Group clay mineralogy, Denver Basin. *Journal of Sedimentary Petrology,* 51(2):541–551. **http://dx.doi.org/10.1306/212F7CCF-2B24-11D7-8648000102C1865D**

Screaton, E.J., Kimura, G., Curewitz, D., and the Expedition 316 Scientists, 2009. Expedition 316 summary. *In* Kinoshita, M., Tobin, H., Ashi, J., Kimura, G., Lallemant, S., Screaton, E.J., Curewitz, D., Masago, H., Moe, K.T., and the Expedition 314/315/316 Scientists, *Proceedings of the Integrated Ocean Drilling Program*, 314/315/316: Washington, DC (Integrated Ocean Drilling Program Management International, Inc.). **http://dx.doi.org/10.2204/iodp.proc.314315316.131.2009**

Środoń, J., Drits, V.A., McCarty, D.K., Hsieh, J.C.C., and Eberl, D.D., 2001. Quantitative X-ray diffraction analysis of clay-bearing rocks from random preparations. *Clays and Clay Minerals*, 49(6):514–528. **http://ccm.geoscienceworld.org/cgi/content/abstract/49/6/514**

Strasser, M., Dugan, B., Kanagawa, K., Moore, G.F., Toczko, S., Maeda, L., Kido, Y., Moe, K.T., Sanada, Y., Esteban, L., Fabbri, O., Geersen, J., Hammerschmidt, S., Hayashi, H., Heirman, K., Hüpers, A., Jurado Rodriguez, M.J., Kameo, K., Kanamatsu, T., Kitajima, H., Masuda, H., Milliken, K., Mishra, R., Motoyama, I., Olcott, K., Oohashi, K., Pickering, K.T., Ramirez, S.G., Rashid, H., Sawyer, D., Schleicher, A., Shan, Y., Skarbek, R., Song, I., Takeshita, T., Toki, T., Tudge, J., Webb, S., Wilson, D.J., Wu, H.-Y., and Yamaguchi, A., 2014a. Expedition 338 summary. *In* Strasser, M., Dugan, B., Kanagawa, K., Moore, G.F., Toczko, S., Maeda, L., and the Expedition 338 Scientists, *Proceedings of the Integrated Ocean Drilling Program,* 338: Yokohama (Integrated Ocean Drilling Program). **http://dx.doi.org/10.2204/iodp.proc.338.101.2014**

Strasser, M., Dugan, B., Kanagawa, K., Moore, G.F., Toczko, S., Maeda, L., Kido, Y., Moe, K.T., Sanada, Y., Esteban, L., Fabbri, O., Geersen, J., Hammerschmidt, S., Hayashi, H., Heirman, K., Hüpers, A., Jurado Rodriguez, M.J., Kameo, K., Kanamatsu, T., Kitajima, H., Masuda, H., Milliken, K., Mishra, R., Motoyama, I., Olcott, K., Oohashi, K., Pickering, K.T., Ramirez, S.G., Rashid, H., Sawyer, D., Schleicher, A., Shan, Y., Skarbek, R., Song, I., Takeshita, T., Toki, T., Tudge, J., Webb, S., Wilson, D.J., Wu, H.-Y., and Yamaguchi, A., 2014b. Site C0002. *In* Strasser, M., Dugan, B., Kanagawa, K., Moore, G.F., Toczko, S., Maeda, L., and the Expedition 338 Scientists, *Proceedings of the Integrated Ocean Drilling Program,* 338: Yokohama (Integrated Ocean Drilling Program). **http://dx.doi.org/10.2204/iodp.proc.338.103.2014**

Tobin, H., Hirose, T., Saffer, D., Toczko, S., Maeda, L., Kubo, Y., Boston, B., Broderick, A., Brown, K., Crespo-Blanc, A., Even, E., Fuchida, S., Fukuchi, R., Hammerschmidt, S., Henry, P., Josh, M., Jurado, M.J., Kitajima, H., Kitamura, M., Maia, A., Otsubo, M., Sample, J., Schleicher, A., Sone, H., Song, C., Valdez, R., Yamamoto, Y., Yang, K., Sanada, Y., Kido, Y., and Hamada, Y., 2015. Expedition 348 summary. *In* Tobin, H., Hirose, T., Saffer, D., Toczko, S., Maeda, L., Kubo, Y., and the Expedition 348 Scientists, *Proceedings of the Integrated Ocean Drilling Program,* 348: College Station, TX (Integrated Ocean Drilling Program). **http://dx.doi.org/10.2204/iodp.proc.348.101.2015**

Tobin, H., Kinoshita, M., Ashi, J., Lallemant, S., Kimura, G., Screaton, E.J., Moe, K.T., Masago, H., Curewitz, D., and the Expedition 314/315/316 Scientists, 2009. NanTroSEIZE Stage 1 expeditions: introduction and synthesis of key results. *In* Kinoshita, M., Tobin, H., Ashi, J., Kimura, G., Lallemant, S., Screaton, E.J., Curewitz, D., Masago, H., Moe, K.T., and the Expedition 314/315/316 Scientists, *Proceedings of the Integrated Ocean Drilling Program,* 314/315/316: Washington, DC (Integrated Ocean Drilling Program Management International, Inc.). **http://dx.doi.org/10.2204/iodp.proc.314315316.101.2009**

Underwood, M.B., Basu, N., Steurer, J., and Udas, S., 2003. Data report: normalization factors for semiquantitative X-ray diffraction analysis, with application to DSDP Site 297, Shikoku Basin. *In* Mikada, H., Moore, G.F., Taira, A., Becker, K., Moore, J.C., and Klaus, A. (Eds.), *Proceedings of the Ocean Drilling Program, Scientific Results,* 190/196: College Station, TX (Ocean Drilling Program), 1–28. **http://dx.doi.org/10.2973/odp.proc.sr.190196.203.2003**

Underwood, M.B., and Guo, J., 2013. Data report: clay mineral assemblages in the Shikoku Basin, NanTroSEIZE subduction inputs, IODP Sites C0011 and C0012. *In* Saito, S., Underwood, M.B., Kubo, Y., and the Expedition 322 Scientists, *Proceedings of the Integrated Ocean Drilling Program,* 322: Tokyo (Integrated Ocean Drilling Program Management International, Inc.). **http://dx.doi.org/10.2204/iodp.proc.322.202.2013**

Underwood, M.B., Saito, S., Kubo, Y., and the Expedition 322 Scientists, 2010. Expedition 322 summary. *In* Saito, S., Underwood, M.B., Kubo, Y., and the Expedition 322 Scientists, *Proceedings of the Integrated Ocean Drilling Program,* 322: Tokyo (Integrated Ocean Drilling Program Management International, Inc.). **http://dx.doi.org/10.2204/iodp.proc.322.101.2010**

Warr, L.N., and Mählmann, R.F., 2015. Recommendations for Kübler Index standardization. *Clay Minerals*, 50(3):283–286. **http://dx.doi.org/10.1180/claymin.2015.050.3.02**

Initial receipt: 28 June 2016
Acceptance: 16 November 2016
Publication: 9 February 2017
MS 338-207

Figure F1. Nankai Trough study area (NanTroSEIZE transect) with locations of Sites C0018 and C0021. White circles = locations of other NanTroSEIZE drill sites along the Kumano transect.

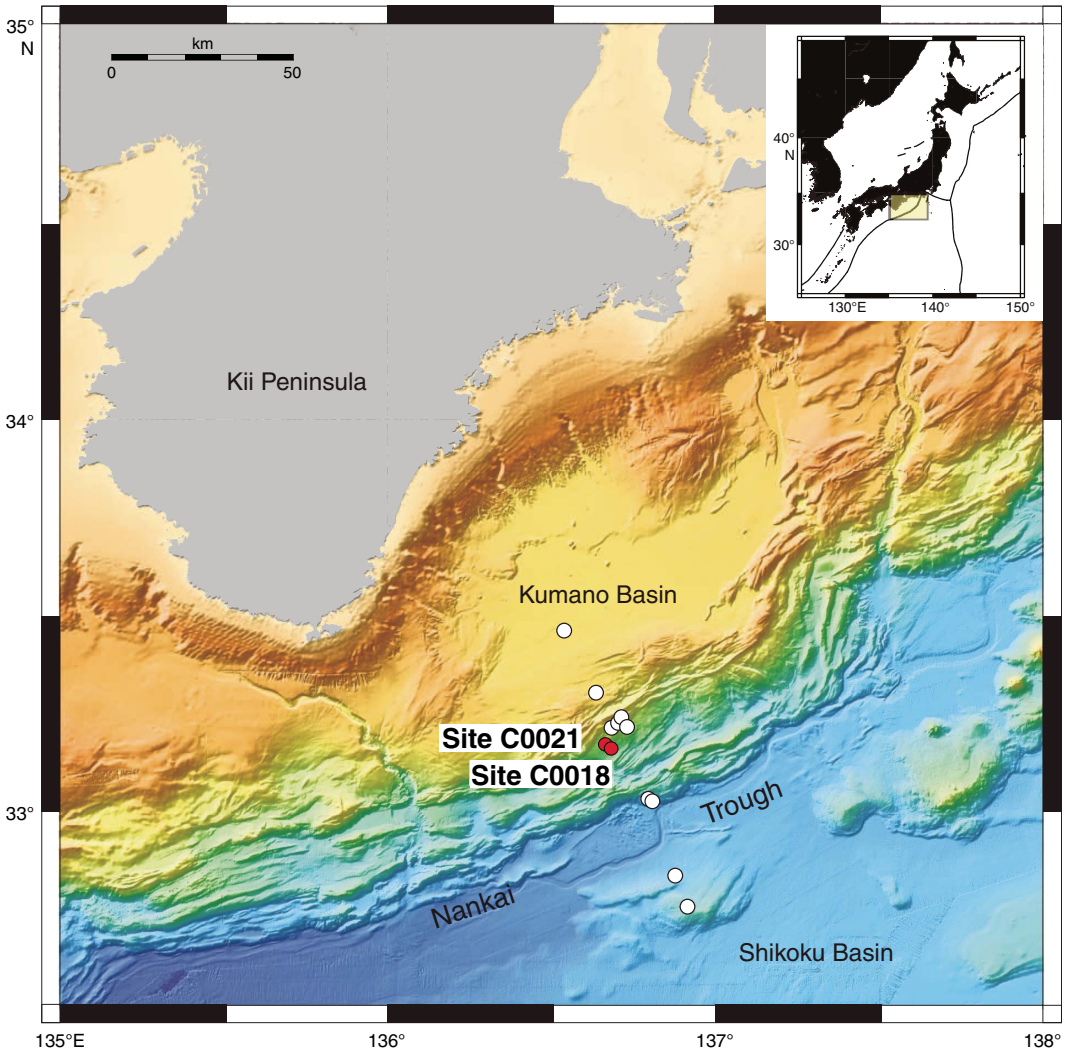

Figure F2. Bathymetry and seismic section crossing the slope basin of Nankai Trough with locations of Sites C0018 and C0021 (see the "Expedition 338 summary" chapter [Strasser et al., 2014a]).

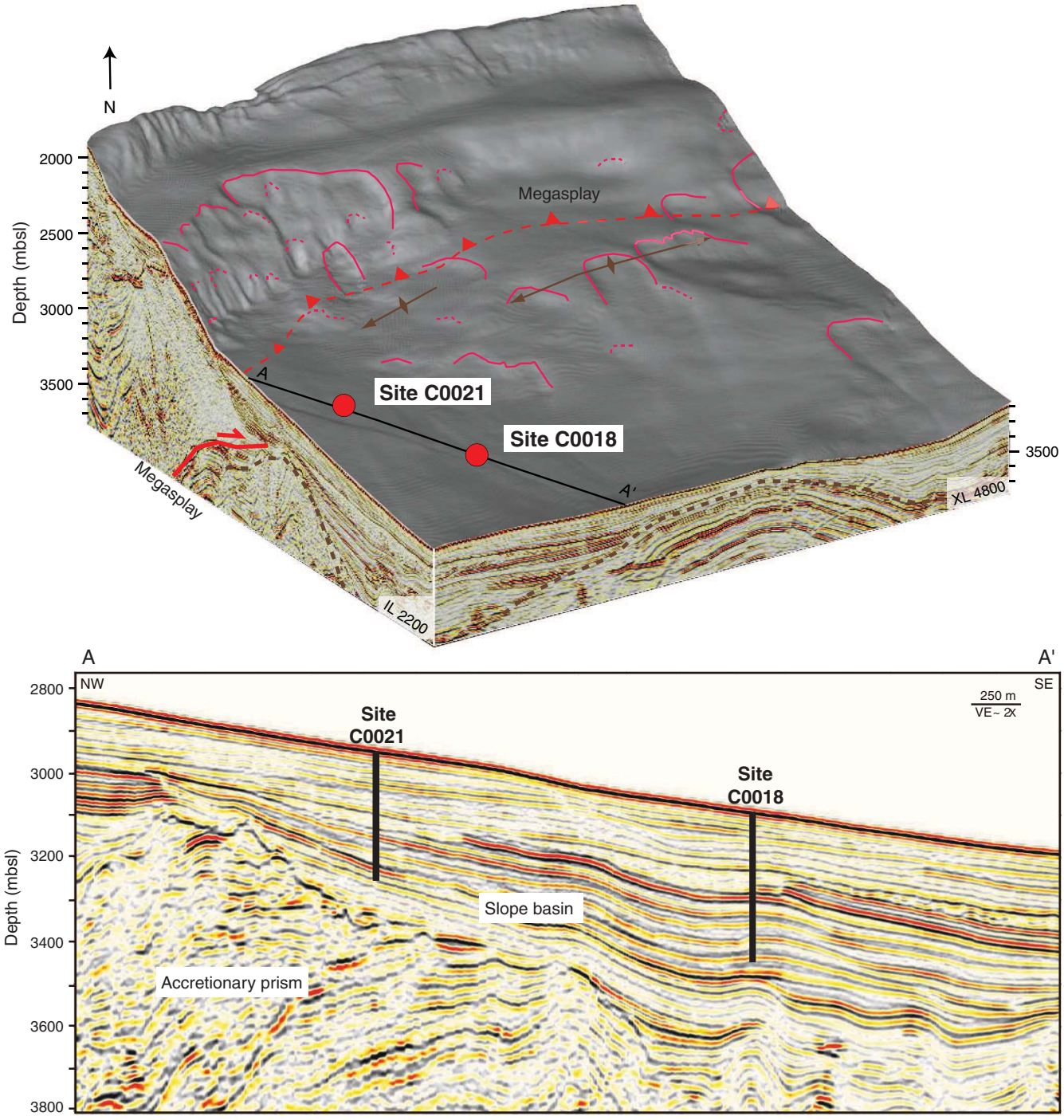

Figure F3. Depth distribution of the calculated relative abundances of smectite, illite, chlorite + kaolinite, and quartz within the clay-size fraction of core samples from Sites C0018 (solid symbols) and C0021 (open symbols) (see the **"Expedition 338 summary"** chapter [Strasser et al., 2014a]).

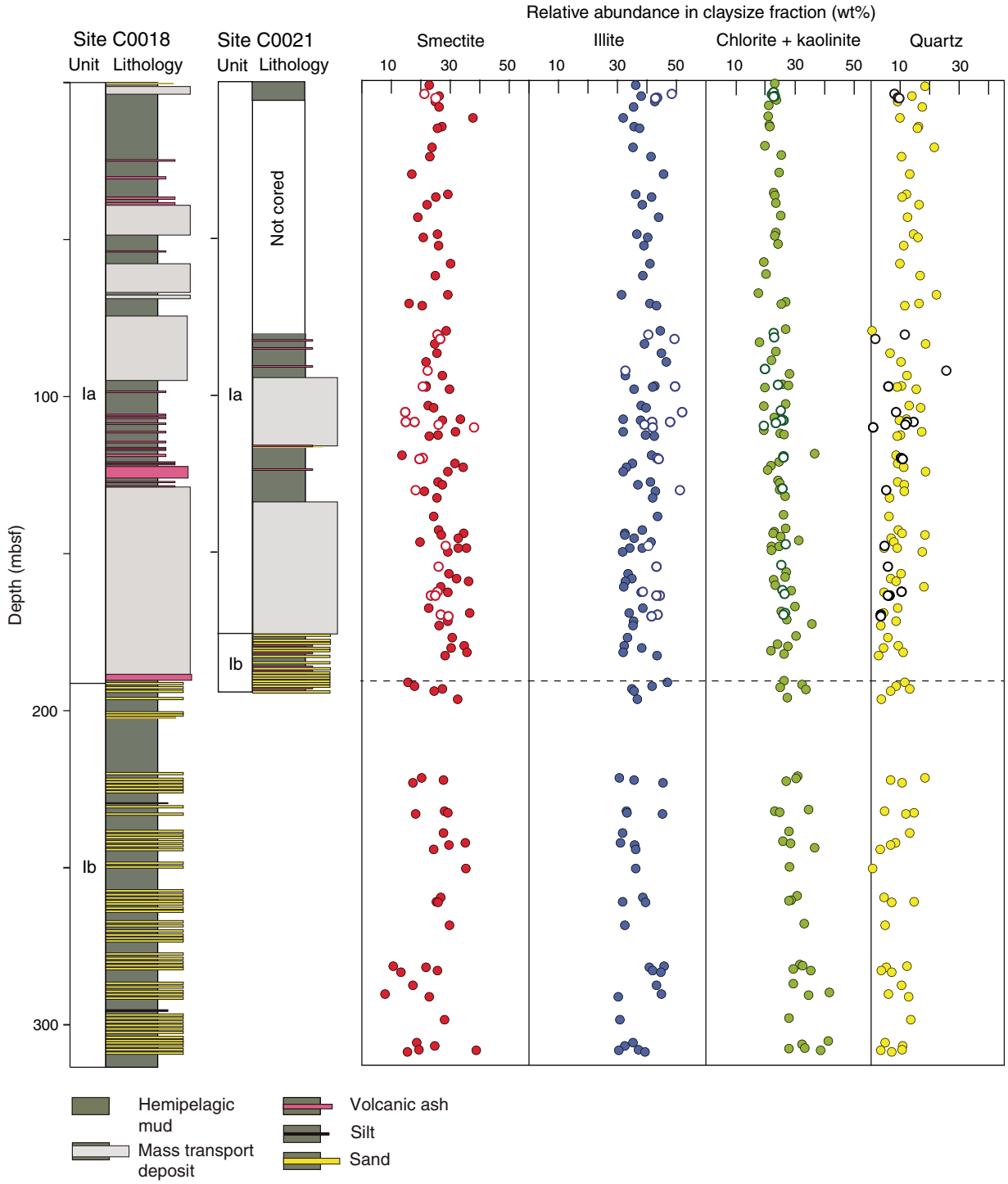

Figure F4. Depth distribution of total clay minerals (Expedition 333 Scientists, 2012b; also see the "Site C0021" chapter [Strasser et al., 2014b]), smectite in bulk sediment, illite in bulk sediment, illite/smectite (I/S) expandability, and illite crystallinity index. Results are from the clay-size fraction of core samples from Sites C0018 (solid symbols) and C0021 (open symbols) (see the "Expedition 338 summary" chapter [Strasser et al., 2014a]). Boundaries for anchizone and epizone metamorphism are from Warr and Mählmann (2015).

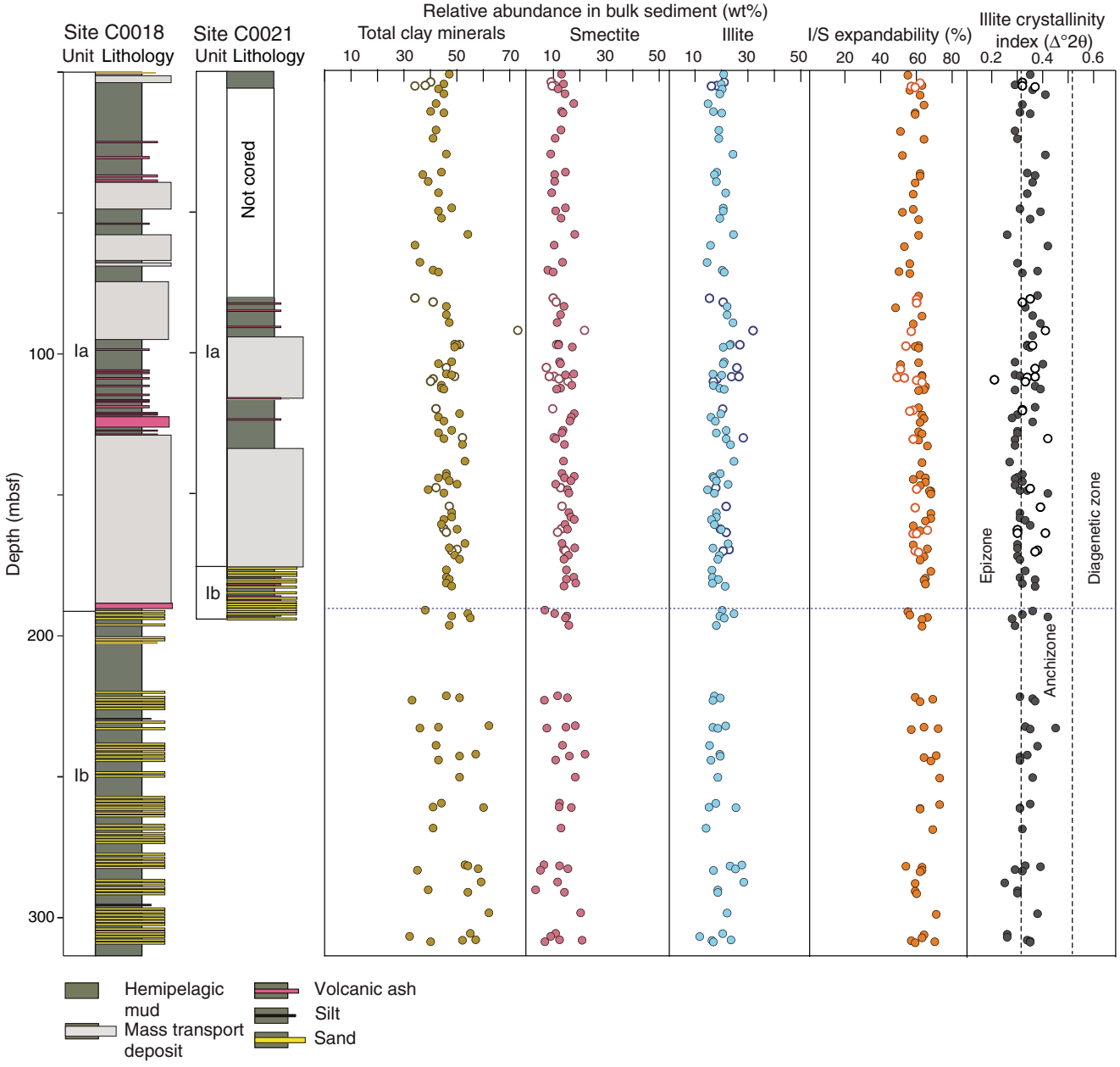

Table T1. Matrix of normalization factors used to calculate relative mineral abundances in clay-size aggregates and derived from singular value decomposition.

Influencing mineral	Target mineral in standard mixture			
	Smectite	Illite	Chlorite	Quartz
Set 1: University of Missouri				
Smectite	0.0003739856	–0.0000289946	–0.0000343775	–0.0000744212
Illite	0.0000427201	0.0012499784	–0.0000283639	0.0000338385
Chorite	–0.0000676622	–0.0000002008	0.0007697485	0.0000524088
Quartz	0.0024368789	0.0009231154	0.0008195109	0.0037061975
Set 2: University of Missouri				
Smectite	0.0003906885	–0.0000299673	–0.0000144669	–0.0000616869
Illite	–0.0001143631	0.0011302975	0.0000131880	0.0000447713
Chorite	–0.0001578547	–0.0000114816	0.0006907853	0.0000047565
Quartz	0.0037122953	0.0014025429	0.0005607141	0.0043742270
Set 3: New Mexico Bureau of Geology and Mineral Resources				
Smectite	0.0007447529	–0.0000319536	–0.0000750672	–0.0001566192
Illite	0.0000631147	0.0037866938	0.0000842230	0.0001176929
Chorite	–0.0003563606	–0.0000673781	0.0025121504	0.0000522907
Quartz	0.0093573136	0.0036491468	0.0032755411	0.0148256450

Table T2. X-ray diffraction analyses results for core samples (<2 µm size fraction), Site C0018. (Continued on next two pages.)

Core, section, interval (cm)	Depth (mbsf)	Integrated peak area (total counts)						I/S mixed-layer clay: Intensity (cps)						Relative abundance in clay-size fraction: SVD normalization factors (wt%)						Biscaye factors (%)*			Relative abundance in bulk sediment (wt%)			
		Smectite (001)	Illite (001)	Kaolinite (001) + chlorite (002)	Quartz (100)	Kaolinite (002) + chlorite (004)	Half peak chlorite (004)	Smectite (001) saddle	Smectite (001) peak	Saddle: peak	I/S expandability (%)	Illite crystallinity index (Δ°2θ)	Set of SVD factors	Smectite	Illite	Kaolinite + chlorite	Quartz	Kaolinite†	Chlorite†	Smectite	Illite	Kaolinite + chlorite	Total clay minerals	Smectite	Illite	Kaolinite + chlorite
333-C0018A-																										
Subunit Ia																										
1H-2, 21	0.98	7,053	4,797	5,059	609	5,487	2,895	181	216	0.84	55	0.35	1	23	36	23	18	0	23	19	53	28	47	13	21	13
1H-6, 22	4.59	1,758	669	575	78	471	252	19	28	0.68	63	0.29	3	26	38	22	14	0	22	31	48	21	45	14	20	11
1H-8, 27	6.24	3,545	1,430	1,203	103	920	447	51	62	0.82	56	0.36	3	25	43	24	9	1	23	30	49	21	43	12	20	11
2H-2, 21	8.06	1,452	565	490	88	473	208	20	28	0.71	62	0.41	3	26	35	21	17	4	18	31	48	21	45	14	19	11
2H-6, 21	11.42	17,960	5,623	6,053	663	4,676	2,270	186	287	0.65	64	0.32	2	38	32	21	10	1	20	34	43	23	42	17	15	10
2H-9, 20	14.27	12,227	6,813	6,804	993	5,607	2,434	212	273	0.78	59	0.31	2	27	36	21	16	4	17	23	51	26	40	13	17	10
2H-11, 8	14.84	9,675	6,016	5,674	801	5,465	2,852	163	210	0.78	59	0.35	2	26	37	21	16	0	21	21	53	25	45	14	20	11
3H-5, 22	20.90	4,908	3,587	3,233	636	2,798	1,375	162	182	0.89	51	0.29	1	24	35	20	22	1	19	19	56	25	42	13	19	10
3H-8, 15	23.71	1,373	599	550	48	499	251	14	21	0.67	64	0.30	3	23	41	25	10	0	25	28	49	23	41	11	19	12
4H-4, 20	29.42	9,098	9,820	8,884	577	8,746	4,283	224	255	0.88	52	0.41	1	17	46	24	13	1	24	14	59	27	46	9	24	13
5H-1, 70	35.80	14,361	6,745	6,948	751	5,506	2,426	155	221	0.70	62	0.34	2	29	36	23	12	4	19	26	49	25	44	15	18	11
5H-2, 20	36.65	3,042	1,235	1,025	103	754	317	40	57	0.70	62	0.37	3	25	42	23	11	5	18	30	49	20	37	10	17	9
5H-4, 21	39.11	10,002	7,574	7,649	978	5,734	2,956	171	220	0.78	59	0.36	2	22	38	23	16	0	23	18	54	28	39	10	18	11
5H-7, 127	43.02	2,496	1,568	1,321	128	1,077	580	46	58	0.79	58	0.34	3	19	44	25	12	0	25	22	55	23	43	9	21	12
6H-4, 21	48.43	15,373	8,756	9,320	1,107	6,474	2,727	261	328	0.80	58	0.31	2	26	37	23	15	5	18	22	51	27	48	14	21	13
6H-5, 124	49.56	6,735	5,351	5,116	491	4,944	2,030	191	215	0.89	52	0.39	1	21	40	23	16	6	17	18	56	27	43	11	21	12
6H-7, 118	52.04	3,454	1,266	1,182	120	981	387	44	61	0.72	61	0.35	3	26	39	24	11	7	17	32	47	22	44	13	19	12
7H-4, 23	57.79	3,070	1,001	714	86	501	183	40	54	0.74	61	0.26	3	30	41	19	10	7	12	36	47	17	54	18	25	11
7H-9, 134	61.65	6,778	4,144	3,634	396	3,231	1,237	176	201	0.88	53	0.42	1	25	39	20	17	6	14	22	54	24	34	10	16	8
8H-6, 21	67.69	9,381	5,480	5,227	1,325	3,820	2,017	200	244	0.82	56	0.30	2	29	31	17	22	0	17	22	52	25	36	13	15	8
8H-9, 37	70.45	4,424	5,632	6,092	572	6,108	2,354	180	199	0.90	50	0.38	1	16	41	27	16	8	18	11	58	31	41	8	20	13
8H-9, 115	71.16	2,882	1,571	1,363	124	1,078	480	49	59	0.83	56	0.32	3	20	43	25	11	4	21	24	53	23	43	10	21	12
9H-5, 64	79.15	8,655	2,665	2,527	67	1,527	809	96	132	0.73	61	0.38	3	29	45	27	0	0	27	36	44	21	—	—	—	—
10H-4, 21	83.32	5,031	3,459	2,595	414	2,158	1,081	176	189	0.93	48	0.33	1	25	39	18	19	0	18	21	58	22	46	14	22	10
10H-7, 63	86.36	3,455	1,357	1,085	72	913	524	33	49	0.67	63	0.36	3	25	45	23	6	0	23	31	49	20	46	12	22	11
10H-9, 87	89.10	2,810	1,502	1,054	101	664	285	53	67	0.79	58	0.39	3	22	46	22	10	4	18	26	55	19	47	11	24	11
11H-4, 26	93.40	1,795	513	675	65	672	292	NR	NR	NR	NR	0.36	3	27	33	28	12	5	23	35	39	26	—	—	—	—
11H-8, 94	96.71	18,384	12,245	11,912	924	8,410	3,818	242	333	0.73	61	0.34	2	22	43	26	10	3	22	20	54	26	49	12	23	14
11H-9, 22	97.13	3,643	1,627	1,627	111	1,287	569	56	73	0.77	59	0.34	3	22	42	28	9	5	23	27	49	24	50	12	23	15
11H-10, 61	97.66	15,702	6,656	6,404	504	6,275	2,913	216	294	0.73	61	0.35	1	30	36	20	15	2	18	28	48	23	49	17	21	11
12H-4, 68	102.88	18,172	11,388	13,275	1,196	8,669	3,848	240	332	0.72	61	0.29	2	22	38	27	13	4	23	20	50	29	48	12	21	15
12H-5, 21	103.56	6,601	4,323	3,523	420	2,601	1,496	190	211	0.90	51	0.40	1	24	40	19	17	0	19	21	56	23	43	13	20	10
12H-8, 120	107.32	26,482	9,530	11,362	1,270	8,516	4,206	280	416	0.67	63	0.29	2	33	32	23	12	0	22	30	44	26	46	17	17	12
12H-9, 20	107.70	4,242	1,359	1,403	121	1,126	452	43	62	0.69	63	0.31	3	27	38	25	10	7	19	34	44	22	48	14	20	13
13H-4, 125	111.37	18,734	6,828	7,147	737	7,076	3,021	198	306	0.65	65	0.37	1	32	32	19	17	4	15	31	45	24	44	17	17	10
13H-5, 108	112.40	3,753	1,357	1,307	116	1,101	383	36	54	0.67	64	0.39	3	26	39	25	10	10	15	32	46	22	44	13	19	12

Table T2 (continued). (Continued on next page.)

Core, section, interval (cm)	Depth (mbsf)	Integrated peak area (total counts): Smectite (001)	Illite (001)	Kaolinite (001) + chlorite (002)	Quartz (100)	Kaolinite (002) + chlorite (004)	Half peak chlorite (004)	I/S mixed-layer clay: Intensity (cps): Smectite (001) saddle	Smectite (001) peak	Saddle: peak	I/S expandability (%)	Illite crystallinity index (Δ°2θ)	Set of SVD factors	Relative abundance in clay-size fraction: SVD normalization factors (wt%): Smectite	Illite	Kaolinite + chlorite	Quartz	Kaolinite†	Chlorite†	Biscaye factors (%)*: Smectite	Illite	Kaolinite + chlorite	Relative abundance in bulk sediment (wt%): Total clay minerals	Smectite	Illite	Kaolinite + chlorite
13H-6, 22	112.67	4,960	2,143	2,000	145	1,676	681	62	85	0.73	61	0.29	3	23	42	26	9	7	19	28	49	23	45	11	21	13
14H-2, 19	118.78	2,839	1,878	2,474	107	1,851	647	51	69	0.74	61	0.37	3	14	42	36	9	15	22	19	49	32	—	—	—	—
14H-4, 20	121.37	31,362	12,258	14,038	1,152	9,831	3,545	302	442	0.68	63	0.30	2	32	35	25	9	9	15	29	45	26	51	18	20	14
14H-5, 21	122.64	25,441	9,180	9,899	1,110	7,053	3,204	266	398	0.67	64	0.28	2	34	33	22	11	3	19	31	45	24	43	17	16	10
14H-6, 128	123.93	12,102	5,029	5,486	664	5,568	2,493	174	244	0.71	62	0.36	1	29	32	21	19	3	18	28	47	25	45	16	18	11
15H-2, 65	127.31	4,802	1,794	1,603	136	1,152	540	60	83	0.72	61	0.30	3	26	41	24	9	2	22	32	47	21	48	14	22	13
15H-3, 33	128.07	5,902	1,925	1,962	199	1,416	633	64	92	0.70	63	0.30	3	27	37	25	11	4	21	34	44	22	43	13	18	12
15H-5, 22	130.27	3,969	2,029	1,752	163	1,386	594	57	78	0.73	61	0.29	3	21	43	25	11	5	20	25	52	22	45	11	22	13
15H-7, 80	132.26	40,689	21,001	21,283	1,160	15,386	6,560	385	635	0.61	66	0.29	2	25	42	26	6	5	21	24	50	25	52	14	23	15
16H-2, 60	138.22	7,093	2,783	2,550	147	1,945	795	77	113	0.68	63	0.27	3	24	44	26	6	7	20	30	48	22	53	14	25	15
16H-11, 12	142.57	4,311	1,463	1,556	121	1,050	428	55	77	0.71	62	0.32	3	26	38	27	9	7	20	32	44	23	46	13	19	13
16H-11, 122	143.66	25,117	8,673	10,032	1,021	7,357	3,052	263	408	0.64	65	0.30	2	35	32	23	11	5	17	31	43	25	46	18	17	12
16H-12, 25	144.10	9,047	4,244	4,956	562	4,990	2,069	174	217	0.80	58	0.29	1	27	32	22	18	5	17	25	47	28	43	14	17	12
17H-1, 50	145.11	37,014	13,709	15,634	1,065	11,414	4,579	359	576	0.62	65	0.32	2	33	36	25	7	7	18	30	45	25	47	16	18	13
17H-2, 39	146.32	4,943	2,261	2,588	135	2,161	806	65	91	0.71	62	0.29	3	20	41	31	8	11	21	26	47	27	50	11	22	17
17H-3, 110	148.28	31,379	10,898	11,429	1,086	8,008	3,327	242	424	0.57	68	0.34	2	35	34	22	9	5	17	32	45	23	39	15	15	9
17H-3, 116	148.34	6,463	1,626	1,636	99	1,412	582	53	91	0.58	67	0.31	3	33	38	25	5	6	19	40	40	20	—	—	—	—
17H-5, 26	149.43	15,757	6,285	7,404	715	7,403	3,233	154	275	0.56	68	0.42	1	29	32	22	17	4	18	28	45	27	45	16	17	12
18H-3, 11	156.35	4,098	1,064	1,324	116	1,034	497	32	57	0.56	68	0.31	3	30	34	27	10	2	26	37	39	24	48	16	18	14
18H-4, 27	157.95	38,202	13,974	17,130	1,083	12,327	5,028	271	481	0.56	68	0.31	2	32	35	26	7	7	20	30	44	27	48	16	18	14
18H-5, 98	158.88	39,096	12,653	14,384	1,302	9,608	3,829	346	552	0.63	65	0.33	2	36	33	23	9	6	16	33	43	24	45	18	16	11
19H-1, 121	160.67	8,947	4,111	5,032	521	4,785	2,445	189	239	0.79	58	0.35	1	27	32	23	18	0	23	25	46	28	44	14	17	12
19H-3, 46	162.39	5,587	1,522	1,780	87	1,157	581	68	95	0.72	62	0.30	3	29	38	29	5	0	29	37	40	23	50	15	20	15
20H-3, 123	167.36	4,250	1,643	1,934	127	1,608	621	64	81	0.79	58	0.30	3	23	39	30	9	9	21	29	45	26	53	13	22	17
20H-5, 21	168.89	42,520	13,241	15,793	875	10,920	4,248	352	569	0.62	66	0.30	2	37	34	25	4	8	18	33	42	25	47	18	17	12
20H-7, 129	171.54	32,915	13,643	17,044	1,182	13,022	6,181	364	544	0.67	64	0.30	2	29	35	27	9	2	25	27	45	28	49	16	19	15
20H-8, 119	172.83	7,290	1,931	3,002	97	2,595	1,330	78	109	0.72	62	0.31	3	26	35	36	3	0	36	35	37	29	51	14	19	19
21H-3, 20	176.79	50,372	17,752	25,982	1,298	17,930	8,336	388	692	0.56	68	0.33	2	31	33	30	6	3	27	29	41	30	46	15	16	15
22H-2, 35	179.26	33,735	11,253	13,621	1,211	9,314	4,123	324	520	0.62	65	0.31	2	35	32	24	9	4	20	32	42	26	46	18	16	12
22H-2, 110	180.01	8,588	2,269	2,554	128	1,859	640	90	136	0.66	64	0.37	3	30	38	27	4	11	16	38	40	22	47	15	19	13
22H-5, 30	181.35	24,256	8,093	9,164	1,021	7,015	3,405	252	396	0.64	65	0.32	2	36	32	22	11	1	21	32	43	24	46	18	16	11
22H-7, 55	182.39	3,965	1,246	1,179	46	990	352	NR	NR	NR	NR	0.37	3	28.1	43.3	26.1	2.5	10.1	16.0	35	44	21	48	14	21	13
										Average:	61	0.332		26.8	37.7	24.2	11.3	4.1	20.2					13.8	19.3	12.3
											Standard deviation:			5.1	4.2	3.6	4.7	3.4	3.8					2.6	2.6	2.0
Subunit Ib																										
24T-1, 36	191.01	3,270	2,657	2,186	179	Barite		61	73	0.84	55	0.36	3	16	47	26	12	Barite		18	58	24	38	7	20	11
24T-2, 20	192.26	4,009	2,096	2,445	129	1,597	665	68	83	0.82	56	0.32	3	18	42	32	9	7	25	23	49	28	54	10	25	19
24T-2, 102	193.08	23,553	10,094	12,380	533	11,743	4,483	242	395	0.61	66	0.42	1	27	35	25	13	8	17	27	46	28	48	15	19	14

Table T2 (continued).

Core, section, interval (cm)	Depth (mbsf)	Integrated peak area (total counts): Smectite (001)	Illite (001)	Kaolinite (001) + chlorite (002)	Quartz (100)	Kaolinite (002) + chlorite (004)	Half peak chlorite (004)	I/S mixed-layer clay: Intensity (cps): Smectite (001) saddle	Smectite (001) peak	Saddle: peak	I/S expandability (%)	Illite crystallinity index (Δ°2θ)	Set of SVD factors	Relative abundance in clay-size fraction: SVD normalization factors (wt%): Smectite	Illite	Kaolinite + chlorite	Quartz	Kaolinite†	Chlorite†	Biscaye factors (%)*: Smectite	Illite	Kaolinite + chlorite	Relative abundance in bulk sediment (wt%): Total clay minerals	Smectite	Illite	Kaolinite + chlorite
24T-3, 27	193.74	44,522	19,612	30,085	1,344	25,587	11,187	536	773	0.69	63	0.28	2	24	36	34	7	6	28	24	43	33	55	14	21	20
24T-5, 114	196.29	9,564	2,252	2,643	131	2,192	723	99	146	0.68	63	0.29	3	32	37	27	4	12	15	40	38	22	47	16	18	13
27T-3, 44	221.37	8,678	5,540	9,410	851	11,886	4,729	185	240	0.77	59	0.31	1	20	31	31	18	9	22	17	45	38	46	11	17	17
27T-3, 116	222.09	43,988	18,088	24,745	1,292	21,756	8,856	318	579	0.55	69	0.36	2	28	36	30	7	8	22	27	44	30	51	15	19	16
27T-4, 66	222.97	3,118	2,061	1,812	136	Barite	Barite	51	72	0.71	62	0.37	3	17	45	27	11	Barite	Barite	21	55	24	33	6	17	10
28T-3, 43	231.90	53,500	19,121	32,196	1,221	24,075	9,527	516	782	0.66	64	0.33	2	28	33	35	5	10	25	28	39	33	62	18	21	22
28T-3, 105	232.52	32,581	12,741	15,240	898	14,095	5,653	182	380	0.48	72	0.45	1	29	33	23	15	6	17	29	45	27	43	15	17	12
28T-4, 26	232.87	1,770	1,186	955	89	Barite	Barite	36	44	0.82	57	0.35	3	18	45	25	12	Barite	Barite	21	56	23	36	7	18	10
29T-1, 68	238.83	19,858	7,491	11,123	392	8,322	2,911	NR	NR	NR	NR	0.38	1	28	32	28	13	11	17	28	42	31	42	13	15	13
29T-4, 52	242.00	1,588	311	405	35	Barite	Barite	8	16	0.50	71	0.34	3	35	31	26	8	Barite	Barite	44	34	22	57	22	19	16
29T-4, 127	242.75	32,166	12,724	16,374	918	12,900	5,781	384	576	0.67	64	0.31	2	29	36	28	7	4	24	28	44	28	51	16	19	15
29T-6, 30	244.05	55,659	22,989	36,955	998	27,614	12,028	402	708	0.57	68	0.31	2	24	36	37	3	7	30	25	42	33	43	11	16	16
30T-2, 104	250.11	72,930	23,394	28,527	835	19,192	7,641	354	764	0.46	73	0.36	2	35	36	28	1	8	20	33	42	26	51	18	19	14
31X-2, 105	259.38	6,826	2,037	2,498	108	Barite	Barite	34	75	0.45	73	0.35	3	27	39	31	5	Barite	Barite	34	41	25	44	12	18	14
31X-4, 31	260.84	22,460	9,655	14,776	758	14,457	5,568	281	399	0.70	62	0.31	1	25	32	29	15	9	20	25	43	33	41	12	15	14
31X-5, 14	260.99	5,953	1,992	2,161	132	1,839	863	73	102	0.72	62	0.31	3	26	39	28	7	2	25	33	44	24	60	17	25	18
32X-2, 17	268.23	42,178	14,416	23,629	983	15,582	6,090	299	550	0.54	69	0.32	2	30	32	33	5	10	23	29	39	32	41	13	14	14
33X-6, 25	281.28	2,142	2,785	2,825	188	2,195	791	47	55	0.85	54	0.33	3	11	46	32	12	12	20	11	59	30	53	6	28	19
33X-7, 31	281.60	34,323	18,166	23,149	859	15,933	6,544	347	503	0.69	63	0.39	2	22	41	32	5	8	24	22	47	30	54	12	23	18
33X-8, 37	282.60	11,099	3,701	4,015	153	3,286	1,213	109	157	0.69	63	0.29	3	26	42	29	4	10	19	33	44	24	58	15	25	18
33X-9, 36	283.13	3,705	2,572	3,031	112	2,632	1,052	53	76	0.70	62	0.32	3	13	45	35	7	10	26	18	51	30	35	5	17	13
34X-2, 19	287.34	2,248	1,374	1,388	95	Barite	Barite	40	52	0.77	59	0.25	3	17	43	29	10	Barite	Barite	21	52	26	59	11	28	19
34X-6, 24	290.17	2,826	2,674	3,690	86	3,067	1,093	51	66	0.77	59	0.30	3	8	45	41	6	16	26	14	51	35	39	3	19	17
34X-7, 83	291.01	17,454	7,431	14,219	435	17,580	6,924	271	363	0.75	60	0.30	1	23	30	34	13	10	24	23	39	38	54	14	19	21
35X-4, 21	298.23	40,999	14,815	22,737	889	20,480	7,849	244	491	0.50	71	0.38	1	28	31	28	14	9	19	28	41	31	62	20	22	20
36X-2, 63	305.55	42,257	20,429	38,423	1,075	34,047	13,346	494	748	0.66	64	0.26	2	19	35	41	5	12	29	21	41	38	55	11	20	24
36X-3, 85	306.62	5,689	1,720	2,630	191	2,299	840	64	92	0.70	63	0.26	3	25	32	32	11	12	21	32	39	30	32	9	12	12
36X-4, 92	307.77	3,533	1,584	2,144	136	1,662	716	67	82	0.82	57	0.34	3	19	37	33	11	6	27	25	45	30	57	12	24	21
36X-4, 110	307.95	55,816	14,664	21,385	1,019	14,233	4,975	358	678	0.53	70	0.35	2	39	30	28	3	11	17	35	37	27	52	21	16	15
36X-5, 24	308.43	5,106	2,618	3,877	141	3,178	1,306	81	105	0.77	59	0.35	3	15	39	39	7	9	29	22	45	33	40	7	17	17
										Average:	63.5	0.33		23.6	37.2	30.7	8.5						12.6	19.5	16.2
												Standard deviation:		7.16	5.29	4.52	4.23						4.63	3.86	3.57

* = Biscaye peak area weighting factors are 1× smectite (001), 4× illite (001), and 2× chlorite (002) + kaolinite (001). † = Proportions of kaolinite and chlorite use the ratio from Guo and Underwood (2011) method and singular value decomposition (SVD) result for undifferentiated chlorite (002) + kaolinite (001). I/S = illite/smectite, cps = counts per step. NR = not resolved, — = no data.

Table T3. Results of X-ray diffraction analyses for core samples (<2 µm size fraction), Site C0021.

		Integrated peak area (total counts)						I/S mixed-layer clay: Intensity (cps)					Relative abundance in clay-size fraction: SVD normalization factors (wt%)						Relative abundance in clay-size fraction: Biscaye factors (%) *			Relative abundance in bulk sediment (wt%)			
Core, section, interval (cm)	Depth (mbsf)	Smectite (001)	Illite (001)	Kaolinite (001) + chlorite (002)	Quartz (100)	Kaolinite (002) + chlorite (004)	Half peak chlorite (004)	Smectite (001) saddle	Smectite (001) peak	Saddle/peak	I/S expandability (%)	Illite crystallinity index (Δ°2θ)	Smectite	Illite	Kaolinite + chlorite	Quartz	Kaolinite†	Chlorite†	Smectite	Illite	Kaolinite + chlorite	Total clay minerals	Smectite	Illite	Kaolinite + chlorite
338-C0021B-																									
Subunit Ia																									
1H-5, 3	3.76	1801	966	648	50	609	240	22	31	0.71	62	0.32	21	48	23	8	7	16	36	56	19	40	9	21	10
1H-5, 120	4.95	2597	1082	837	76	513	170	47	58	0.81	57	0.32	25	43	23	9	10	13	40	50	19	38	10	18	10
1H-6, 23	5.17	2527	1039	796	77	524	307	39	50	0.78	59	0.37	25	43	23	10	0	23	41	50	19	34	10	16	9
2H-2, 27	80.40	2169	854	689	79	461	124	35	46	0.76	60	0.35	26	40	23	12	13	9	41	49	20	34	10	15	9
2H-3, 18	81.71	5580	2118	1490	53	779	293	71	94	0.76	60	0.32	26	49	23	2	8	15	44	50	17	41	11	21	10
3H-4, 18	91.82	859	617	486	153	401	208	25	31	0.81	57	0.41	22	33	20	26	0	20	28	57	23	73	22	32	19
3H-8, 88	96.93	3460	1850	1312	75	1050	366	65	76	0.86	54	0.36	21	50	24	6	10	14	35	55	19	51	11	27	13
4H-6, 19	105.07	2753	2423	1660	109	1359	581	64	71	0.90	51	0.37	15	52	25	9	5	20	25	61	21	46	7	26	13
4H-8, 32	108.09	2320	1630	1439	160	1026	393	58	63	0.92	49	0.37	18	42	26	14	8	18	27	56	25	49	10	24	15
4H-8, 35	108.12	1637	1551	1143	108	716	433	41	47	0.87	53	0.34	15	48	25	12	0	25	23	61	23	49	8	26	14
5H-1, 60	109.07	3725	1389	1217	136	875	402	57	75	0.76	60	0.21	26	39	23	12	3	21	42	47	21	41	12	18	11
5H-2, 4	109.81	9488	2196	1594	88	1023	416	101	147	0.69	63	0.33	38	42	19	1	5	14	56	41	15	40	15	17	8
6H-3, 18	119.66	3022	1564	1350	112	940	385	48	61	0.79	58	0.32	21	43	26	10	6	19	34	52	23	42	10	20	12
6H-4, 25	120.05	3059	1757	1487	128	1001	420	60	73	0.82	56	0.32	19	44	26	11	6	20	32	54	23	—	—	—	—
7H-4, 3	129.86	4217	2523	1837	83	1207	547	72	91	0.79	58	0.42	18	51	26	5	3	22	33	56	20	52	10	28	14
9H-2, 18	147.62	6206	1864	1863	100	1374	548	80	107	0.75	60	0.35	28	40	27	5	7	19	45	43	21	42	13	18	12
9H-7, 70	154.12	5714	2065	1789	108	1110	619	81	106	0.76	59	0.39	26	43	25	6	0	25	43	47	20	47	13	22	13
10H-8, 19	162.22	3523	1266	1231	113	788	344	26	43	0.60	66	0.30	26	39	26	10	5	21	41	46	22	45	13	20	13
10H-9, 110	163.42	4999	2082	1819	107	NP	NP	70	89	0.79	58	0.41	23	44	26	6	NP	NP	39	49	21	46	11	22	13
10H-9, 110	163.42	4985	1872	1696	96	1229	596	66	87	0.76	60	0.30	25	43	26	6	1	25	41	47	21	—	—	—	—
11H-5, 13	169.44	4607	1552	1425	61	1114	631	66	86	0.77	59	0.38	27	44	27	3	0	27	44	45	21	50	14	23	14
12H-2, 0	169.99	5399	1590	1512	71	1033	468	65	88	0.74	61	0.37	29	42	26	3	3	23	47	43	20	48	15	21	13
										Average:	58.2	0.35	23.6	43.7	24.3	8.4	4.8	19.5				11.7	21.6	12.0
										Standard deviation:			5.2	4.5	2.1	5.3	3.8	4.5				3.2	4.3	2.7

* = Biscaye peak area weighting factors are 1× smectite (001), 4× illite (001), and 2× chlorite (002) + kaolinite (001). † = Proportions of kaolinite and chlorite use the ratio from Guo and Underwood (2011) method and singular value decomposition (SVD) result for undifferentiated chlorite (002) + kaolinite (001). I/S = illite/smectite, cps = counts per step. NP = no peak, — = no data.